JACS
JOURNAL OF THE AMERICAN CHEMICAL SOCIETY

COMMUNICATION

pubs.acs.org/JACS

Hydrothermal Etching Assisted Crystallization: A Facile Route to Functional Yolk-Shell Titanate Microspheres with Ultrathin Nanosheets-Assembled Double Shells

Wei Li, Yonghui Deng,* Zhangxiong Wu, Xufang Qian, Jianping Yang, Yao Wang, Dong Gu, Fan Zhang, Bo Tu, and Dongyuan Zhao*

Department of Chemistry, Shanghai Key Laboratory of Molecular Catalysis and Innovative Materials, and Laboratory of Advanced Materials, Fudan University, Shanghai 200433, P. R. China

Supporting Information

ABSTRACT: We report a facile "hydrothermal etching assisted crystallization" route to synthesize Fe_3O_4@titanate yolk-shell microspheres with ultrathin nanosheets-assembled double-shell structure. The as-prepared microspheres possess a uniform size, tailored shell structure, good structural stability, versatile ion-exchange capability, high surface area, large magnetization, and exhibit a remarkable catalytic performance.

Hollow colloidal particles have recently been subjected to extensive research for their unique characteristics such as high surface area, low density, and potential applications in catalysis, controlled release, and lithium-ion batteries.[1] More recently, to endow hollow particles with multifunctionalities and synergetic properties, considerable effort has been devoted to rational design of the shells with desirable components and unique structures, and functionalize the interior spaces through encapsulating functional species,[2−6] namely, creating yolk-shell structures with both hollow space, functional interior core and useful outer shell.

So far, numerous approaches based on template-assisted process,[3,4] Kirkendall[5] or Ostwald ripening effect,[6] and one-step surfactant-involved strategy[2] have been developed to synthesize yolk-shell structures; however, most are composed of a single-layer shell. Multishelled yolk-shell structures can provide a chance to create sophisticated functionalities through introducing different guest species into selective chambers.[7] Lou and co-workers have reported the synthesis of double-shelled SnO_2 yolk-shell structures based on a hydrothermal shell-by-shell deposition method.[8] Wu and co-workers have demonstrated a layer-by-layer method to produce multishelled SiO_2 yolk-shell structures.[9] To the best of our knowledge, almost all existing methods for yielding multiple shells are exclusively based on the layer-by-layer strategy.[1a] Moreover, the shells are generally composed of aggregated nanoparticles. Very little success has been achieved to construct the shells with anisotropic building blocks, such as one-dimensional (1D) nanowires, naotubes, and 2D nanosheets.[3f] In addition, although remarkable progress has been made in the synthesis of yolk-shelled catalysts with an active core and a protective shell, there is rarely effective work to *in situ* produce the active catalysis sites, especially acid sites, on the shell. It is well-known that such heterogeneous acid catalysts are easy to handle and applicable for designing "green" catalytic process.

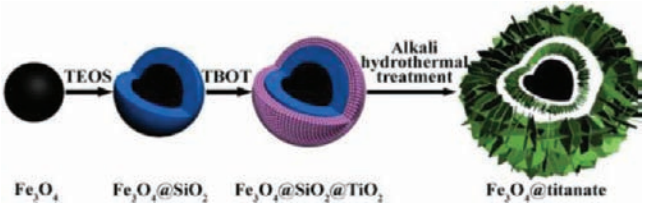

Figure 1. Schematic illustration of the formation process of the Fe_3O_4@titanate double-shelled yolk-shell microspheres.

Therefore, it remains a grand challenge to develop a new strategy for fabricating yolk-shell structures with both multishells, built-in shell functionalities, and especially unique shell structures.

Here, we demonstrate a facile "hydrothermal etching assisted crystallization" route to produce Fe_3O_4@titanate double-shelled yolk-shell microspheres. To our knowledge, this is the first report on synthesizing this unique structure with double shells constructed by 2D ultrathin nanosheets, which intrinsically possess active acid sites. The sol−gel process of tetraethyl orthosilicate (TEOS) and tetrabutyl titanate (TBOT) was explored to coat SiO_2 and TiO_2 on uniform Fe_3O_4 nanoparticles in turn, giving rise to a typical sandwich structure (Fe_3O_4@SiO_2@TiO_2). During hydrothermal treatment in an alkaline solution, the SiO_2 interlayer was first etched, followed by concurrent but separate TiO_2 layer-etching and epitaxial titanate nanosheets-growth. In this case, the SiO_2 layer not only promotes the coating of TiO_2, but also acts as the template for the first cavity. The TiO_2 layer provides two interfaces for the nucleation and discrete space for simultaneously self-assembled nanosheets-growth along opposite directions, and *in situ* acts as the template for the second cavity. In this way, the yolk-shell structure with nanosheets-assembled double shells is formed. The inclusion of Fe_3O_4 cores allows the convenient separation and recycling by applying external magnetic fields.[10] The designed yolk-shell microspheres possess a uniform size, tailored shell structure, good structural stability, versatile ion-exchange capability, high surface area, large magnetization, and exhibit a remarkable catalytic performance.

The synthesis procedure involves three steps (Figure 1). First, uniform magnetite particles were coated with silica through classical Stöber method using TEOS as a precursor. Second,

Received: June 15, 2011
Published: September 09, 2011

ACS Publications © 2011 American Chemical Society

dx.doi.org/10.1021/ja2055287 | *J. Am. Chem. Soc.* 2011, 133, 15830–15833

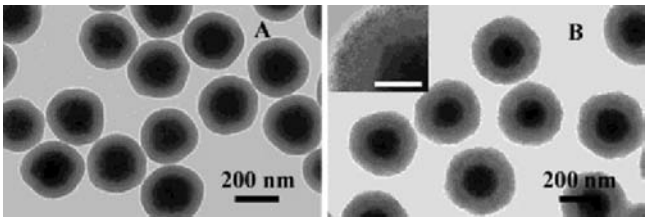

Figure 2. TEM images of the (A) Fe_3O_4@SiO_2 and (B) Fe_3O_4@SiO_2@TiO_2 microspheres. The inset in B is a magnification TEM image and the scale bar is 100 nm.

the resulted Fe_3O_4@SiO_2 microspheres were further coated with titania through a facile sol−gel approach using TBOT as a precursor. Third, the obtained Fe_3O_4@SiO_2@TiO_2 microspheres were hydrothermally treated in NaOH solution (1.0 M) at 150 °C, leading to the formation of Fe_3O_4@titanate double-shelled yolk-shell microspheres.

The magnetite particles were prepared via a solvothermal method as described previously.[10b] The obtained Fe_3O_4 particles possess uniformly spherical shape and a mean diameter of ∼180 nm (Figure S1). The particles show excellent dispersibility in polar solvents because of numerous citrate groups anchored on the surface, which favors the subsequent coating with silica and titania. Fe_3O_4@SiO_2 microspheres obtained after the first sol−gel process show a relatively smooth surface with a diameter of ∼280 nm (Figure S2a). TEM image indicates that the thickness of the SiO_2 layer is ∼50 nm (Figure 2A). The further sol−gel process leads to the formation of Fe_3O_4@SiO_2@TiO_2 microspheres (Figure S2b) with a diameter of ∼340 nm, indicating the presence of ∼30 nm thick TiO_2 layer. The Fe_3O_4@SiO_2@TiO_2 microspheres possess rough surface compared with Fe_3O_4@SiO_2 microspheres (Figure S2 inset). It may be attributed to the fact that TBOT undergoes hydrolysis and condensation faster than TEOS, thus, yielding the large nanoclusters of titania. TEM images (Figure 2B) further confirm the rough surface and the typical sandwich structure, where obvious contrast of the rough titania-layer, gray silica-interlayer, and dark magnetite core can be clearly visible.

After the hydrothermal treatment in NaOH solution (1.0 M) at 150 °C, unique flower-like microspheres with a uniform size of ∼560 nm are obtained (Figure 3a). The X-ray diffraction (XRD) pattern of the obtained microspheres (Figure S3) shows the characteristic broad diffraction peaks, which can be indexed to the layered titanates and Fe_3O_4 particles, respectively.[11,10b] It suggests the amorphous titania experiences a localized crystallization process during the hydrothermal treatment. A magnification FESEM image (Figure 3b) clearly reveals that the microspheres are composed of numerous ultrathin nanosheets with bottom edges pointing toward the center. The slight curl and self-attachment of the nanosheets result in the highly open and stable structure. TEM observations (Figure 3c,d) clearly indicate that the microspheres possess a unique yolk-shell structure, where a dark particle encapsulated in two separated gray layers and the self-assembled nanosheets can be clearly elucidated. The mean shell thicknesses of the outer and inner layer are estimated to be around ∼110 and ∼40 nm, respectively. Furthermore, the double-shelled structure is also verified from the broken microspheres (Figure S4). High-resolution TEM (HRTEM) image (Figure 3e) clearly shows that the nanosheets are the lamellar structures with a *d*-spacing of ∼0.8 nm, consistent with the XRD results (Figure S3). The layer number

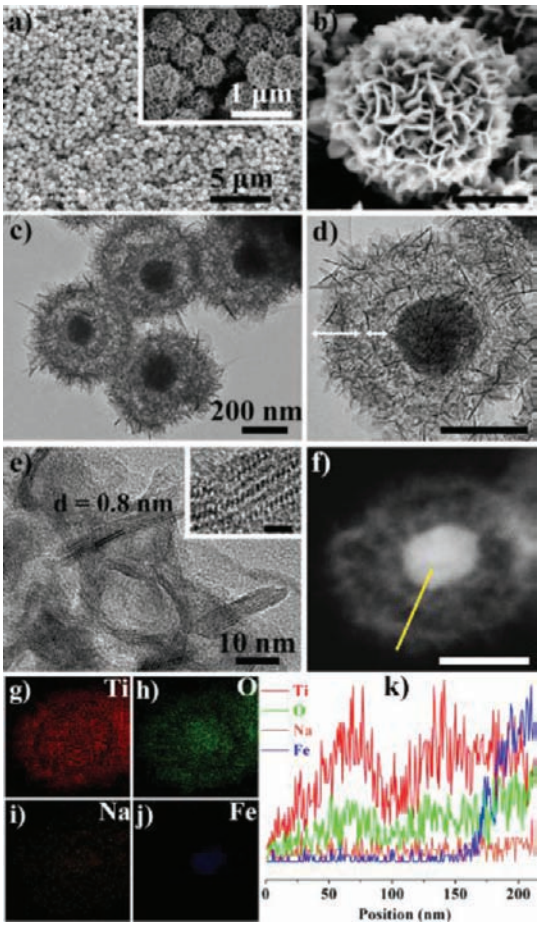

Figure 3. The obtained Fe_3O_4@titanate double-shelled yolk-shell microspheres: (a) FESEM images (inset is the magnification FESEM image, which clearly shows the ultrathin-nanosheets self-assembled structure), (b) the FESEM image of a single sphere, (c and d) TEM images, (e) HRTEM images (the scale bar of the inset is 1 nm), and (f) the STEM image; the scale bars in b, d, and f are all 200 nm. (g−j) EDX elemental maps of Ti, O, Na, and Fe, respectively, (k) line scanning profiles of Ti, O, Na, and Fe recorded along the line shown in f.

of each nanosheet varies in the range of 2−6. A magnification HRTEM image (Figure 3e inset) clearly reveals three monolayers, which are relative to the edge-sharing TiO_6 octahedra and the interlayer Na ions, endowing the versatile ion-exchange capability.[12] Generally, the lamellar nanosheets formed during the alkaline hydrothermal treatment are very unstable and spontaneously roll into tubular structures driven by excess surface energy.[12] The remarkable ultrathin nanosheets obtained in this study are probably caused by the *in situ* crystallization and self-attachment of them on the interface between TiO_2 and the alkali solution. The scanning TEM (STEM) image of a single yolk-shell microsphere after the H^+-exchange, combined with EDX elemental mapping and line scanning (Figure 3f−k), clearly reveals the double-shelled yolk-shell structure with a magnetite core and titanate double shells. The integrated energy dispersive X-ray spectroscopy (EDS) analysis (Figure S5) further confirms the presence of Ti, Fe, O, and neglectable amount of Na and Si. The atomic ratio of Ti and Fe is calculated to be ∼2.56, which is consistent with the results (the atomic ratio of Ti/Fe = ∼2.44, ∼0.48 wt % for Na and ∼0.12 wt % for Si) determined from the elemental analysis by inductively coupled plasma-atomic

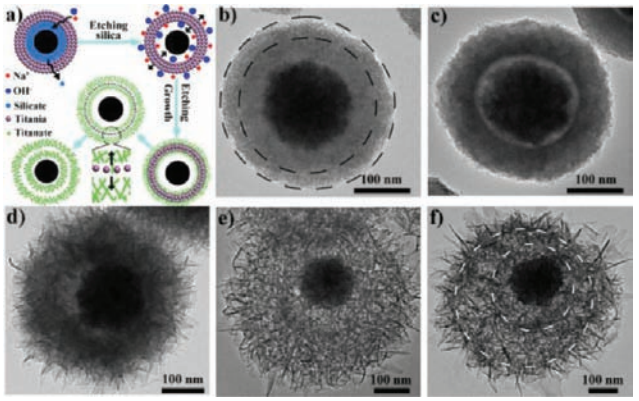

Figure 4. (a) Schematic illustration of the "hydrothermal etching assisted crystallization" strategy for the formation of the Fe_3O_4@titanate double-shelled yolk-shell microspheres. TEM images of a single sphere synthesized at 150 °C with hydrothermal treatment time: (b) 0 min, (c) 20 min, (d) 2 h, (e) 12 h, and (f) 24 h.

emission spectrometry (ICP-AES). The results indicate that Si species are almost completely removed after the hydrothermal treatment, resulting in Fe_3O_4@titanate double-shelled yolk-shell microspheres with versatile ion-exchange capability.

The magnetic properties of the pristine Fe_3O_4 particles and Fe_3O_4@titanate microspheres were investigated using a superconducting quantum interference device (SQUID) magnetometer (Figure S6). Both the samples show the typical hysteresis loops with no detectable remanence or coercivity, reflecting a superparamagnetic property. The magnetization saturation values of the Fe_3O_4 particles and Fe_3O_4@titanate microspheres are 63.7 and 17.7 emu/g, respectively. The Fe_3O_4 content of Fe_3O_4@titanate microspheres is calculated to be ~28 wt %, consistent with the EDX and ICP results. As a result of the superparamagnetic property and high magnetization, the yolk-shell microspheres in their homogeneous dispersion show fast motion to the applied magnetic field. Once the magnetic field is removed, they can be quickly redispersed into homogeneous suspension upon a slight shake. This trait enables the efficient separation and purification, and facilitates their wide applications. N_2 sorption measurements show that the yolk-shell microspheres have a nanoporous structure (Figure S7), derived from the packing of the nanosheets in the shells. It exhibits a type-IV isotherm with a type-H1 hysteresis loop. The pore size distribution derived from the adsorption branch by using the Barrett–Joyner–Halenda (BJH) model indicates a mean pore size of ~7.5 nm. The BET surface area and total pore volume are calculated to be ~150 m^2/g and ~0.27 cm^3/g, respectively.

To gain insight into the formation of the Fe_3O_4@titanate double-shelled yolk-shell microspheres (Figure 4a), time-dependent experiments were carried out. After the hydrothermal treatment at 150 °C for 20 min, the typical sandwich structure (Figure 4b) was converted to a yolk-shell structure (Figure 4c, Figure S8a) with no obvious change on the TiO_2 layer (Figure S9a,b). Compared with the XRD patterns of the parent Fe_3O_4@SiO_2@TiO_2 microspheres, the characteristic diffraction peak from amorphous silica is absent in the obtained products (Figure S10). After continuous hydrothermal treatment for 2 h, the shells of the microspheres were found to be composed of ultrathin nanosheets (Figure 4d, Figure S8b). As time was prolonged to 12 h (Figure 4e, Figure S8c) and 24 h (Figure 4f), well-developed yolk-shell structure with nanosheets-assembled double shells are formed. TEM images indicate that the diameters of the inner-shell and inward-diameter of the outer shell (circled in Figure 4f) are ~265 and ~360 nm, consistent with the inner (280 nm) and outer one (340 nm) of the amorphous TiO_2 layer (circled in Figure 4b), respectively. That clearly indicates that the titanate-nanosheets grow oppositely along the surface of TiO_2 layer, accompanied by some structure shrinkage. Further prolonging the reaction time (48 h), nanosheets tend to roll into nanotubes driven by the weak attachment interactions and the excess surface energy (Figure S11). With this interesting structural evolution, the entire microsphere size increases from ~340 to ~560 nm (Table S1) with increasing hydrothermal treatment time; however, the thickness of the nanosheet shows no obvious change (Figure S9c,d and Figure 3e). The intensities of diffraction peaks from titanate (Figure S10) gradually become stronger from 0 min to 24 h, further demonstrating that the nanosheets grow longer with prolonging treatment time.

On the basis of the above observations, we propose a "hydrothermal etching assisted crystallization" strategy for the formation of the Fe_3O_4@titanate double-shelled yolk-shell microspheres (Figure 4a). The high concentration NaOH solution (1.0 M) first can etch the amorphous silica layer at the beginning of the reaction, resulting in hollow titania micrsopheres encapsulated magnetite particles (the first cavity). The porous structure of the TiO_2 shells helps the alkali solution permeate conveniently and enables the formation of relatively high alkali concentration along the inner and outer interface, which facilitates the consequent nucleation. As the reaction progresses, the amorphous TiO_2 layer starts to be etched. Simultaneously, the epitaxial titanate nanosheets-growth which occurs as the result of heterogeneous nucleation is energetically favored over the homogeneous one.[4f] It should be noted that the two interfaces and separated space make the nanosheets grow along the opposite directions, and the TiO_2 layer-dissolution *in situ* produces the second cavity. The stable structure strongly relies on spontaneous self-assembly of the 2D ultrathin nanosheets into 3D hierarchical spheres, which reduces the surface energy and prevents them from wrapping or collapse. The further titania-etching and titanate-growth may be facilitated through Ostwald ripening.[6] Obviously, as the hydrothermal reaction proceeds, the TiO_2 layer can be eventually dissolved and the titanate nanosheets grow longer along independent directions, thereby creating the double-shelled yolk-shell structure. However, further prolonging the reaction time could increase the length of the nanosheets but decrease the self-attachment interaction, resulting in nanotubular strcuture. Therefore, by simply controlling the hydrothermal treatment time, the shell structure can be effectively tuned from single layer to double layers, meanwhile the building block of each layer varies from 0D nanoparticles to 2D nanosheets and 1D nanotubes.

The magnetic separability and unique yolk-shell structure with high surface area and highly open pores make the Fe_3O_4@titanate microspheres ideal candidates for catalysis application. The catalytic performance of the Fe_3O_4@titanate microspheres was tested for the Friedel–Crafts (FC) alkylation of toluene with benzylchloride, and compared with that of conventional solid acid catalysts (Table S2). The Fe_3O_4@titanate microspheres show a high conversion of 97.1% with a selectivity of 54% toward *p*-benzyltoluene, which is better than other acid catalysts such as niobic acid, zeolites, and SO_4^{2-}/ZrO_2, due to the lagre pore and high surface area. The result is comparable with protonated titanate nanotubes.[13a] The excellent performance may be attributed to: (1) the high porosity and hollow structure, which are

beneficial for the transportation and adsorption of large molecules thus, promoting the catalytic process; (2) the ultrathin nanosheets structures, which enable a maximized molecular diffusion and make active sites exposed to reactants; (3) the synergic effect between Lewis and Brønsted acid sites of titanates, which plays an important role in alkylation.[13] To investigate the reusability, the Fe_3O_4@titanate microspheres were easily recovered by a magnet from the catalytic reaction solution. The catalyst exhibits a similar catalytic performance without visible reduction even after running for more than 8 cycles (Figure S12). Interestingly, the Fe_3O_4@-titanate microspheres can be *in situ* converted to Fe_3O_4@*NS*-TiO_2 microspheres with Fe_3O_4 core and anatase TiO_2 nanosheet shell through simple annealing (Figure S13a). The double-shelled yolk-shell structure were well retained (Figure S13b). The Fe_3O_4@*NS*-TiO_2 microspheres show an excellent photocatlytic activity toward Rhodamine B with a rate constant of 0.072 min^{-1}, which is faster than that of P25 TiO_2 (0.042 min^{-1}, Figure S13c). Because of the magnetic core, the catalysts can be easily recycled and exhibit approximately constant activity even after 10 cycles (Figure S13d). The high porosity and ultrathin nanosheets structures of Fe_3O_4@*NS*-TiO_2 microspheres offer more active sites,[14] which are responsible for the excellent performance.

In summary, we have demonstrated a facile "hydrothermal etching assisted crystallization" strategy to synthesize Fe_3O_4@-titanate yolk-shell microspheres with ultrathin nanosheets-assembled double-shell structure. The obtained Fe_3O_4@titanate microspheres possess a uniform size ($\sim$ 560 nm), tailored shell structure, good structural stability, versatile ion-exchange capability, highly surface area (150 m^2/g), large magnetization (17.7 emu/g), and enhanced acid catalysis performance for Friedel–Crafts alkylation. The corresponding Fe_3O_4@*NS*-TiO_2 derivatives show excellent photocatalytic activeity. This facile synthesis strategy can be easily extended to design other multifunctional yolk-shell materials, such as Au@titanate, Fe_2O_3@ titanate and CNTs@titanate, and their correspongding titania derivatives.

■ ASSOCIATED CONTENT

Supporting Information. Detailed experimental procedures, characterization methods, SEM images, XRD data, EDX data, N_2 sorption results, TEM images and catalytic performance measurements. This material is available free of charge via the Internet at http://pubs.acs.org.

■ AUTHOR INFORMATION

Corresponding Author
yhdeng@fudan.edu.cn; dyzhao@fudan.edu.cn

■ ACKNOWLEDGMENT

We greatly appreciate financial support from the National Science Foundation (20890123 and 21073040) and the State Key Basic Research Program of China (2009AA033701 and 2009CB930400) and Science & Technology Commission of Shanghai Municipality (08DZ2270500) and Shanghai Leading Academic Discipline Project (B108).

■ REFERENCES

(1) (a) Caruso, F.; Caruso, R. A.; Mohwald, H. *Science* **1998**, *282*, 1111. (b) Vriezema, D. M.; Aragones, M. C.; Elemans, J.; Cornelissen, J.; Rowan, A. E.; Nolte, R. J. M. *Chem. Rev.* **2005**, *105*, 1445. (c) Lou, X. W.; Archer, L. A.; Yang, Z. C. *Adv. Mater.* **2008**, *20*, 3987. (d) Zhang, Q.; Wang, W. S.; Goebl, J.; Yin, Y. D. *Nano Today* **2009**, *4*, 494.

(2) (a) Liu, J.; Qiao, S. Z.; Hartono, S. B.; Lu, G. Q. *Angew. Chem., Int. Ed.* **2010**, *49*, 4981. (b) Wu, X. J.; Xu, D. S. *J. Am. Chem. Soc.* **2009**, *131*, 2774.

(3) (a) Lee, J.; Park, J. C.; Song, H. *Adv. Mater.* **2008**, *20*, 1523. (b) Arnal, P. M.; Comotti, M.; Schuth, F. *Angew. Chem., Int. Ed.* **2006**, *45*, 8224. (c) Kim, M.; Sohn, K.; Bin Na, H.; Hyeon, T. *Nano Lett.* **2002**, *2*, 1383. (d) Kamata, K.; Lu, Y.; Xia, Y. N. *J. Am. Chem. Soc.* **2003**, *125*, 2384. (e) Tan, L. F.; Chen, D.; Liu, H. Y.; Tang, F. Q. *Adv. Mater.* **2010**, *22*, 4885. (f) Chen, J. S.; Chen, C. P.; Liu, J.; Xu, R.; Qiao, S. Z.; Lou, X. W. *Chem. Commun.* **2011**, 2631.

(4) (a) Chen, Y.; Chen, H. R.; Guo, L. M.; He, Q. J.; Chen, F.; Zhou, J.; Feng, J. W.; Shi, J. L. *ACS Nano* **2010**, *4*, 529. (b) Ikeda, S.; Ishino, S.; Harada, T.; Okamoto, N.; Sakata, T.; Mori, H.; Kuwabata, S.; Torimoto, T.; Matsumura, M. *Angew. Chem., Int., Ed.* **2006**, *45*, 7063. (c) Kim, J. Y.; Yoon, S. B.; Yu, J. S. *Chem. Commun.* **2003**, 790. (d) Kim, S. H.; Yin, Y. D.; Alivisatos, A. P.; Somorjai, G. A.; Yates, J. T. *J. Am. Chem. Soc.* **2007**, *129*, 9510. (e) Van Gough, D.; Wolosiuk, A.; Braun, P. V. *Nano Lett.* **2009**, *9*, 1994. (f) Zhang, T. R.; Ge, J. P.; Hu, Y. X.; Zhang, Q.; Aloni, S.; Yin, Y. D. *Angew. Chem., Int. Ed.* **2008**, *47*, 5806.

(5) (a) Yin, Y. D.; Rioux, R. M.; Erdonmez, C. K.; Hughes, S.; Somorjai, G. A.; Alivisatos, A. P. *Science* **2004**, *304*, 711. (b) Gao, J. H.; Liang, G. L.; Zhang, B.; Kuang, Y.; Zhang, X. X.; Xu, B. *J. Am. Chem. Soc.* **2007**, *129*, 1428.

(6) Li, H. X.; Bian, Z. F.; Zhu, J.; Zhang, D. Q.; Li, G. S.; Huo, Y. N.; Li, H.; Lu, Y. F. *J. Am. Chem. Soc.* **2007**, *129*, 8406.

(7) (a) Liu, J.; Hartono, S. B.; Jin, Y. G.; Li, Z.; Lu, G. Q.; Qiao, S. Z. *J. Mater. Chem.* **2010**, *20*, 4595. (b) Li, G. L.; Shi, Q.; Yuan, S. J.; Neoh, K. G.; Kang, E. T.; Yang, X. L. *Chem. Mater.* **2010**, *22*, 1309.

(8) (a) Lou, X. W.; Yuan, C. L.; Archer, L. A. *Small* **2007**, *3*, 261. (b) Lou, X. W.; Yuan, C. L.; Archer, L. A. *Adv. Mater.* **2007**, *19*, 3328.

(9) Wu, X. J.; Xu, D. S. *Adv. Mater.* **2010**, *22*, 1516.

(10) (a) Deng, Y.; Qi, D.; Deng, C.; Zhang, X.; Zhao, D. *J. Am. Chem. Soc.* **2008**, *130*, 28. (b) Liu, J.; Sun, Z. K.; Deng, Y. H.; Zou, Y.; Li, C. Y.; Guo, X. H.; Xiong, L. Q.; Gao, Y.; Li, F. Y.; Zhao, D. Y. *Angew. Chem., Int. Ed.* **2009**, *48*, 5875.

(11) (a) Liu, J. H.; Chen, J. S.; Wei, X. F.; Lou, X. W.; Liu, X. W. *Adv. Mater.* **2011**, *23*, 998. (b) Yuan, Z. Y.; Zhou, W. Z.; Su, B. L. *Chem. Commun.* **2002**, 1202.

(12) (a) Bavykin, D. V.; Friedrich, J. M.; Walsh, F. C. *Adv. Mater.* **2006**, *18*, 2807. (b) Bavykin, D. V.; Walsh, F. C. *Eur. J. Inorg. Chem.* **2009**, 977.

(13) (a) Kitano, M.; Nakajima, K.; Kondo, J. N.; Hayashi, S.; Hara, M. *J. Am. Chem. Soc.* **2010**, *132*, 6622. (b) Li, S. H.; Zheng, A. M.; Su, Y. C.; Zhang, H. L.; Chen, L.; Yang, J.; Ye, C. H.; Deng, F. *J. Am. Chem. Soc.* **2007**, *129*, 11161. (c) Lin, C. H.; Chien, S. H.; Chao, J. H.; Sheu, C. Y.; Cheng, Y. C.; Huang, Y. J.; Tsai, C. H. *Catal. Lett.* **2002**, *80*, 153.

(14) (a) Son, J. S.; Wen, X. D.; Joo, J.; Chae, J. S.; Baek, S.; Park, K.; Kim, J. H.; An, K. J.; Yu, J. H.; Kwon, S. G.; Choi, S. H.; Kuk, Y.; Hoffmann, R.; Hyeon, T. *Angew. Chem., Int. Ed.* **2009**, *48*, 6861. (b) Son, J. S.; Yu, J. H.; Kwon, S. G.; Lee, J.; Joo, J.; Hyeon, T. *Adv. Mater.* **2011**, *23*, 3214.